

## Chapter 5

### Dynamic Phase Control

#### 5.1 Introduction

The study of coherent control to manipulate molecular systems has generated numerous tools that can be useful for directing a system under optical, especially ultrafast, excitation[12, 13, 22, 26, 32, 50-57]. The tools of coherent control may be applicable to quantum computing, where superpositions of quantum states, or qubits, are used to perform computational operations[58]. Crucial to being able to perform quantum operations is the ability to manipulate individual states within qubits. Basic computations have been performed on spin systems using Nuclear Magnetic Resonance with considerable success[59-62]. Optically manipulated systems using trapped atoms and ions also show promise for quantum computation by using narrow bandwidth lasers to resonantly control particular transitions between states[63, 64]. Wide bandwidth, ultrafast pulses have been proposed as a means to implement quantum computational operations using the relatively dense states inherent to single quantum dots and even molecules[32, 54-57]. Given the relatively short decoherence times ( $<100$  ns) of these more complex systems, the use of ultrafast laser sources is valuable to perform sufficient numbers of operations for meaningful computations. This chapter explores a mechanism for using ultrafast pulse shaping techniques to manipulate individual states in a molecular superposition, specifically multiple

rotational states in an excited electronic state of the lithium dimer. As an example of using nonresonant frequencies to control the amplitude of molecular rotational states, a transient Z-gate is implemented. Using an ultrafast pulse with sufficient bandwidth to encompass resonant transitions to two excited states, one state of the two state superposition will have its sign unchanged while the other will undergo a sign inversion. The operation is transient in nature, so it can not be used for actual computation, but the results illustrate new possibilities of using optical pulse shaping techniques for individual state manipulation.

In the previous chapter, it has been shown that resonant frequencies can be used to control the phases of states involved in a wave packet[7, 48], and it has also been shown that nonresonant frequencies can be used to transiently manipulate the absolute amplitude of resonant transitions, even in the weak field [33, 65]. One additional aspect of transient, ultrafast control of wave packet phases has not been demonstrated: *i. e.* the transient phase of a wave packet can be controlled by using nonresonant frequencies. As in any first order process, though, the final wave packet phase and amplitude at long times are determined by the resonant frequencies, as is expected[12]. This will be demonstrated by observing the coherence only portions of the signal as written out in Eq. (4.4c)

We show in this chapter that the wave packet phase can be induced to undergo a  $\pi$  phase shift at time zero relative to long times. Assuming that one contributing state in the superposition has a constant phase at all times, the signal shows a change in sign because of a transient sign inversion of the second state. This dynamics is accomplished by summing resonant and nonresonant

contributions with the same sign for one state while summing resonant and nonresonant contributions with opposite sign for the other. The amplitudes of the relative contributions of each effect are manipulated so that the nonresonant contribution dominates at short times for the opposite sign but disappears at long times. This process of inverting the sign of one state of a superposition while leaving the second unaltered is characteristic of a quantum computational Z-gate, which in this case is constructed in a transient fashion.

This example of controlling the dynamic phase of a wave function in the weak field regime provides a rather clear illustration of the limitations and possibilities of precise control of molecular systems. As long as the intensity of the electric field is weak enough to disregard intensity dependent Rabi oscillation effects, pure phase shaping of the ultrafast pulses fully controls the dynamics of the effects observed. In Sec. 5.2, a theoretical framework for these experiments is presented using first-order perturbation theory. In Sec. 5.3 is presented a categorization of the resonant and nonresonant effects that are used as tools in these experiments. Finally, experimental results are presented, discussed, and quantified in Sec. 5.4.

## 5.2 Theory

This chapter develops a method to induce a transient sign change in one state of a two state superposition, or wave packet, using language consistent with the formalisms of quantum computing. The wave packet consists of two states that are excited coherently, so that:

$$\Psi'(t) = c_0(t)|0\rangle + c_1(t)|1\rangle + c_2(t)|2\rangle, \quad (5.1a)$$

where  $c_0(t)$  is the launch state wavefunction amplitude,  $c_1(t)$  and  $c_2(t)$  are the complex excited state wavefunction amplitudes to be described below, and  $|0\rangle$ ,  $|1\rangle$  and  $|2\rangle$  are the time dependent rovibrational wavefunctions [*i. e.*  $|1(R, \theta, t)\rangle = |1(R, \theta)\rangle e^{i\omega_1 t}$ ] in the superposition [see Fig. 5.1]. The detection scheme is only sensitive to  $|1\rangle$  and  $|2\rangle$ , so the effective wave packet can be reformulated as

$$\Psi(t) = c_1(t)|1\rangle + c_2(t)|2\rangle. \quad (5.1b)$$

As described previously[33, 48], the photoionization signal using parallel, linear pump and probe polarizations can be written as

$$S(t) \equiv |pr_1|^2 |c_1(t)|^2 + |pr_2|^2 |c_2(t)|^2 + 2|pr_1 pr_2| |c_1(t)c_2(t)| \cos[\Delta\omega t + \Delta\phi(t)], \quad (5.2)$$

where the only change from Eq. (4.4a) is the explicit time dependence of  $\Delta\phi(t)$ . Since the multiphoton ionization pathway from the launch state ( $pr_0$ ) is weak,  $pr_0 \ll pr_1, pr_2$ , so all launch state terms are left out of the signal, and the time dependent signal only shows the dynamics of the excited states.

In these experiments, the probe step consists of an ultrafast pulse of a different color (645 nm) than the pump pulse (801 nm) [33] so as to avoid any ambiguities in the contributions to the signal when the probe comes before the pump. With the 645 nm probe pulse, the probability for a probe-pump (*i. e.*,  $t < 0$ ) ionization pathway is below the noise level, allowing time dependent ionization to occur only at positive time delays. This allows the transient populations and coherent oscillations to be measured reliably around  $t=0$ .

In Eq. (5.2), the  $c_n(t)$  factors have the same functional form as Eq. (4.2), with nonresonant contributions to the coefficient being  $\pm\pi/2$  out of phase with

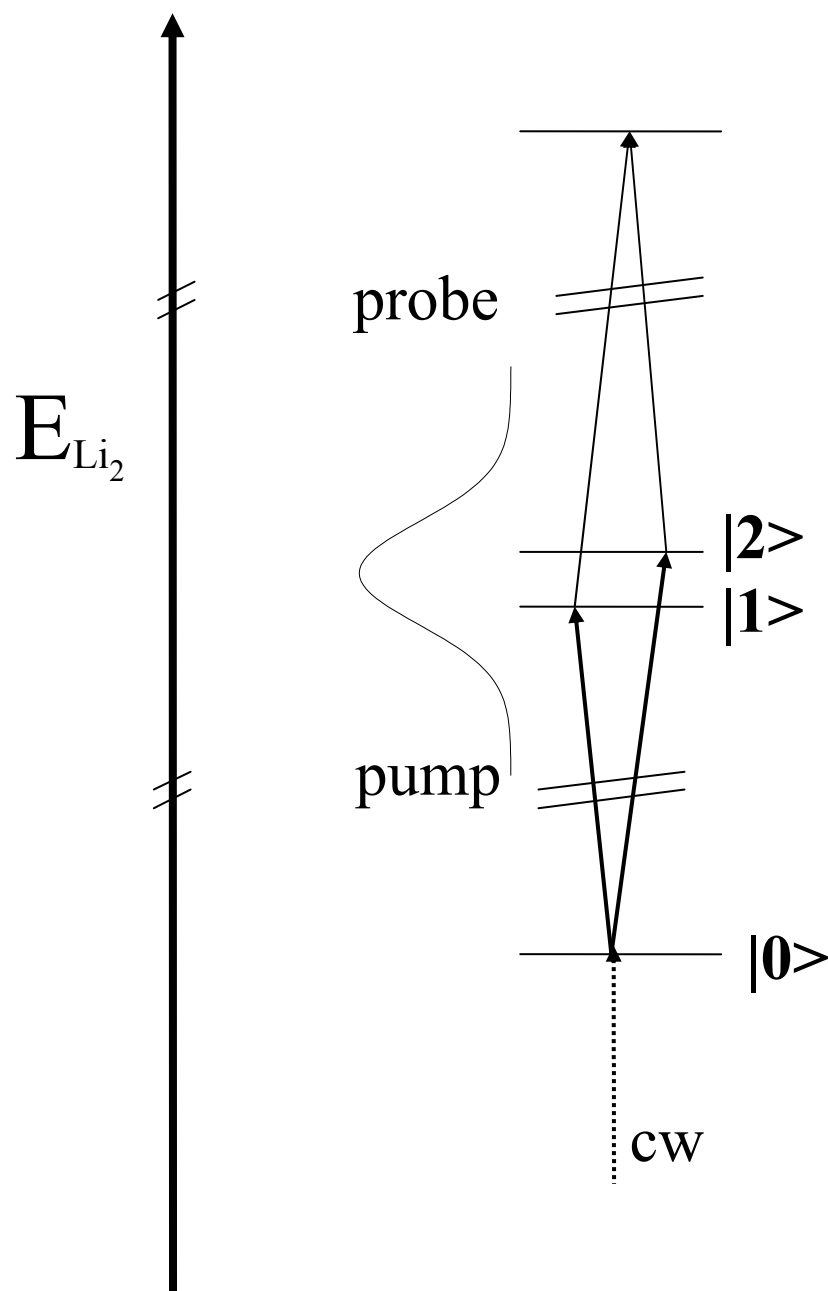


Figure 5.1. States involved in excitation scheme. A cw laser excites from the X electronic state to a pure launch state (state  $|0\rangle$ ) on the A electronic state. A wide bandwidth 801 nm ultrafast pump pulse excites a superposition of states (states  $|1\rangle$  and  $|2\rangle$ ) on the E electronic state, which is subsequently ionized by a time delayed 645 nm ultrafast probe pulse.

respect to the resonance and with a  $1/\Delta$  dependence. Notice that these effects result in a complex amplitude  $c_n(t)$ , which under the conditions imposed in these experiments will remain primarily real. The manner in which the various contributions interact is explored in the next section where it is demonstrated how to change the wavefunction sign.

In this chapter, a transformation of the qubit in Eq. (5.1b) is mathematically equivalent to a quantum computational Z-gate. Using a matrix formulation, the action of the ultrafast pulse on the prepared superposition transforms the system as a single qubit Z-gate:

$$\begin{bmatrix} c_1(f) \\ c_2(f) \end{bmatrix} \approx \begin{bmatrix} 1 & 0 \\ 0 & -1 \end{bmatrix} \begin{bmatrix} c_1(i) \\ c_2(i) \end{bmatrix}. \quad (5.3)$$

First, a superposition is prepared such that at  $t=0.0$  ps, the two excited states have amplitudes of opposite sign so that  $c_1 \approx 1$ , and  $c_2 \approx -1$ . The electric field then drives the system so that the sign of  $c_2$  changes, leaving  $c_2=1$ . Although this transformation can be analyzed in terms of a series of three correlated pulses (*i.e.* pulses with a defined relationship between the carrier frequency phases), it will be explained in terms of the spectral contributions to the signals, as given in Eq. (4.2).

### 5.3 Experiment

In the experiments described in this chapter, the experimental setup is the same as chapter 4. What are varied are the pulse shapes that are investigated as well as the analysis of the data. As a result, this section will focus on the basics of different

types of excitation mechanisms and pulse shapes, as if they were simply experimental tools.

To investigate phase mask effects, the available spectrum is defined as consisting of two spectral channels separated at the energetic midpoint between the two resonant transitions. A global phase offset can be added to the channel for state  $|2\rangle$  in order to control the long time wave packet phase. Within each channel, *i. e.* for each state, resonant and nonresonant contributions to the excited state wave function coefficient are independently controlled. See Fig. 5.2 for one phase mask that is used to add the resonant and nonresonant contributions of the excited state coefficients along with the corresponding observed time domain evolution. In Fig. 5.2a, it is shown that a small bandwidth region around each resonance ( $\sim 8 \text{ cm}^{-1}$  each) is assigned a phase halfway between the positive and negative detuned nonresonant frequencies. The effect of these narrow bandwidth regions is a monotonic increase in the excited state coefficient, as shown by the triangles in Fig. 5.2b, taken with magic angle probe so there are no wave packet recurrences. This will be referred to as the resonant contribution. The applied  $\pi$  phase shift between positive and negative detuned frequencies around each resonance compensates for the intrinsic spectroscopic  $\pi$  phase shift of the nonresonant contributions above and below the resonances. This allows the nonresonant contributions to cooperate on short timescales, as seen by the circles in Fig. 5.2b. The solid line in Fig. 5.2b gives  $|c_1(t)|^2 + |c_2(t)|^2$ , which has been normalized. Assuming that the crosstalk between control channels for the two coefficients is insignificant [see previous chapter][33], which is achieved when

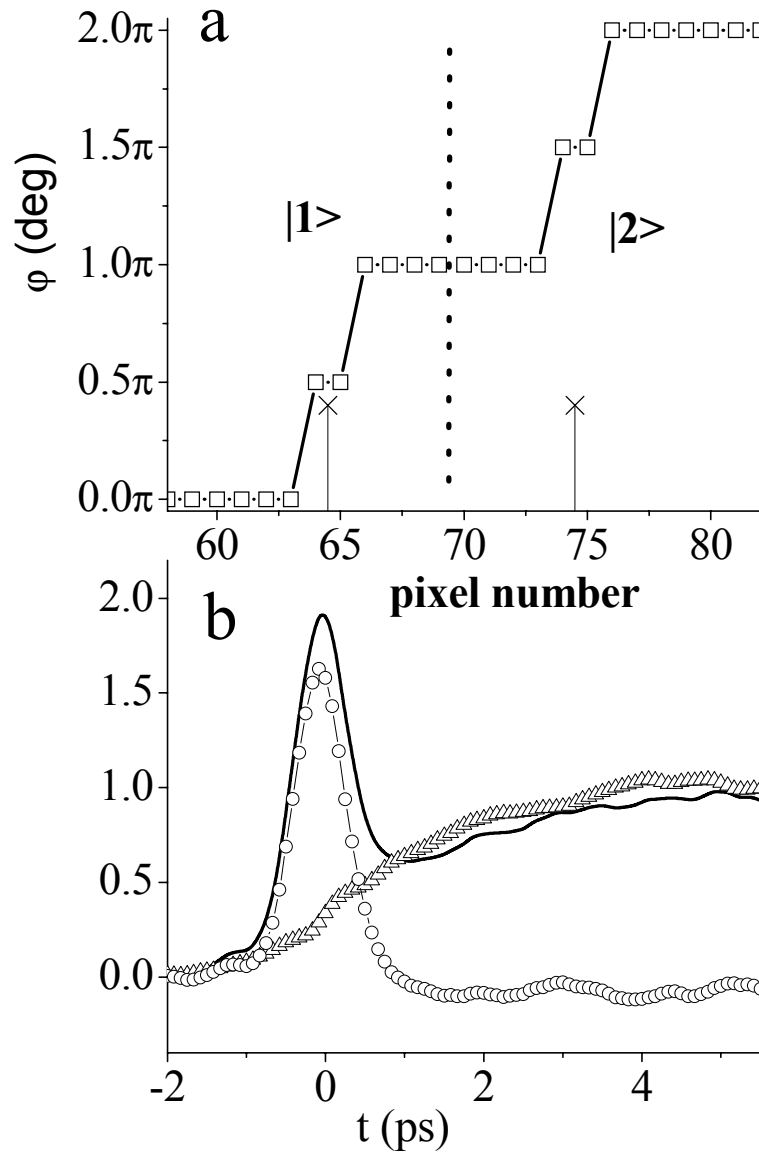


Figure 5.2. Phase shaped population transfer traces. Panel a: Phase mask used to maximize population transfer at  $t=0.0$  ps. The applied phase mask is given by ( $\square$ ), and resonances are marked with (X). The applied phase masks near each resonance (*i. e.* in each channel) are identical, assuring that both states follow the same excitation pathway. Panel b: Magic angle traces (to suppress the rotational quantum beats) using the applied phase mask of panel a. The solid line represents the total population transfer signal, the ( $\triangle$ ) shows the resonant only contribution, and the ( $\circ$ ) gives the nonresonant contribution, which is just the difference between the two traces.

the two resonances are spaced far apart energetically,  $|c_1(t)| \approx |c_2(t)|$ . By taking the square root of the signal and renormalizing, a measure of each coefficient is obtained. This signal shows that at the times of interest in this paper,  $t=0$  and  $t=\infty$ ,  $|c_1(t)| = 1.4$  and  $1.0$ , respectively. This information will be used later to quantify the manipulations of coefficient  $c_2(t)$ .

Figure 5.3 is a schematic diagram of the signed *amplitude* [*i.e.*,  $c_n(t)$ , not  $|c_n(t)|^2$ ] of the excited state coefficients. The traces in Fig. 3a-b are calculated from parameters of the square root of the cooperative signal as described above. Given that these contributions add to yield the amplitude of  $c_n(t)$ , the resonant and nonresonant effects within each channel can be subtracted as well as added. This is done by multiplying either the resonant or nonresonant contribution by  $-1$ . Fortuitously, in the complex plane, multiplication by  $-1$  is identical to the addition of  $\pi$  phase, which is accomplished by the application of  $\pi$  phase to the appropriate pump wavelengths. As can be seen in the modeled coefficients in Fig. 5.3b, simply subtracting the nonresonant contribution from the resonant gives a value of  $-0.7$  for  $c_2(0)$ . In these experiments, state  $|1\rangle$  is manipulated to be a sum of the resonant and nonresonant contributions with the same sign, while state  $|2\rangle$  consists of a sum of contributions with opposing signs. Since the coefficient for  $|2\rangle$  reflects a difference, the absolute amplitude of this negative coefficient can be increased in one of two ways: by increasing the negative part or by decreasing the positive part. Here, the positive contribution due to the resonant frequencies has been time shifted by  $1.0$  ps by applying a simple linear phase mask to the resonant regions [solid line in Fig. 5.3a] with the nonresonant contribution unaltered. To

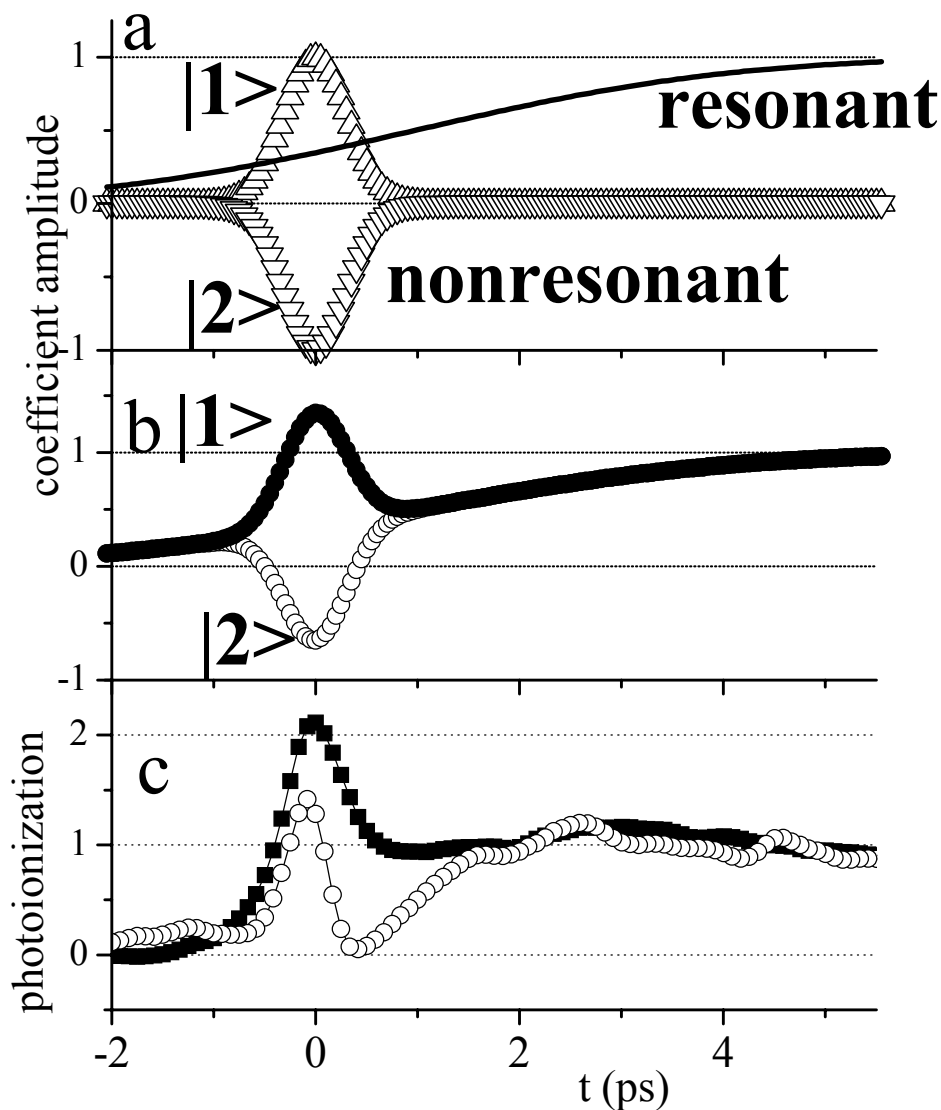


Figure 5.3. Resonant/nonresonant interaction scheme for inducing sign inversion. Panel a: Calculated resonant and nonresonant contributions to the population transfer. The solid line is the resonant contribution time shifted by 1.0 ps. The ( $\Delta$ ) and ( $\nabla$ ) reflect the nonresonant contribution for states  $|1\rangle$  and  $|2\rangle$ , respectively, when inducing a sign inversion. Panel b: Total excited state coefficient evolution using contributions from panel a. The ( $\bullet$ ) show the time evolution for state  $|1\rangle$ , and ( $\circ$ ) shows the time evolution for state  $|2\rangle$ . Panel c: Experimental photoionization traces for a single state with a phase mask that adds resonant and nonresonant contributions ( $\blacksquare$ ), and a phase mask that subtracts the resonant and nonresonant contributions ( $\circ$ ). Note that the photoionization correlates with the square of the amplitude coefficients.

demonstrate the effects experimentally, each type of phase mask was applied to a pulse exciting the  $v_E, J_E=7, 39$  state, and the results are shown in Fig. 5.3c. The light near state  $v_E, J_E=7, 41$ , spaced over  $62 \text{ cm}^{-1}$  away, was attenuated to make sure that it was not excited. Excitation with the additive phase mask shows the expected transient peak at  $t=0.0$  ps. Excitation with the subtractive phase mask shows the photoionization goes nearly to zero at  $0.42$  ps. It is at this time that the sign of the coefficient inverts and the phase quickly changes. These traces show the total photoionization, so they actually reflect  $|c(t)|^2$ , but it is quite clear from the data that the subtractive phase mask changes the coefficient sign of this isolated state.

#### 5.4 Results and Discussion

To serve as a reference, a case where the dynamics of the population transfer is controlled identically for both states involved in the wave packet is shown in Fig. 5.4 {see [33]}. Here, the resonant and nonresonant contributions to the signal are added together with the same sign for both states  $|1\rangle$  and  $|2\rangle$ . The upper part of Fig. 5.4a shows that there is a peak in the excited state coefficients at  $t=0.0$  ps. The difference between the full signal and the excited state coefficient signal yields purely the coherence signal, which is shown as the circles in the lower part of Fig. 5.4a. This is obtained from parallel and magic angle pump-probe polarization signals, respectively. Notice that the coherence signal only appears after the excited state coefficients become nonzero (*i.e.* after  $t=-1.0$  ps), and that it has an overall constant temporal phase of  $\pi$  radians.

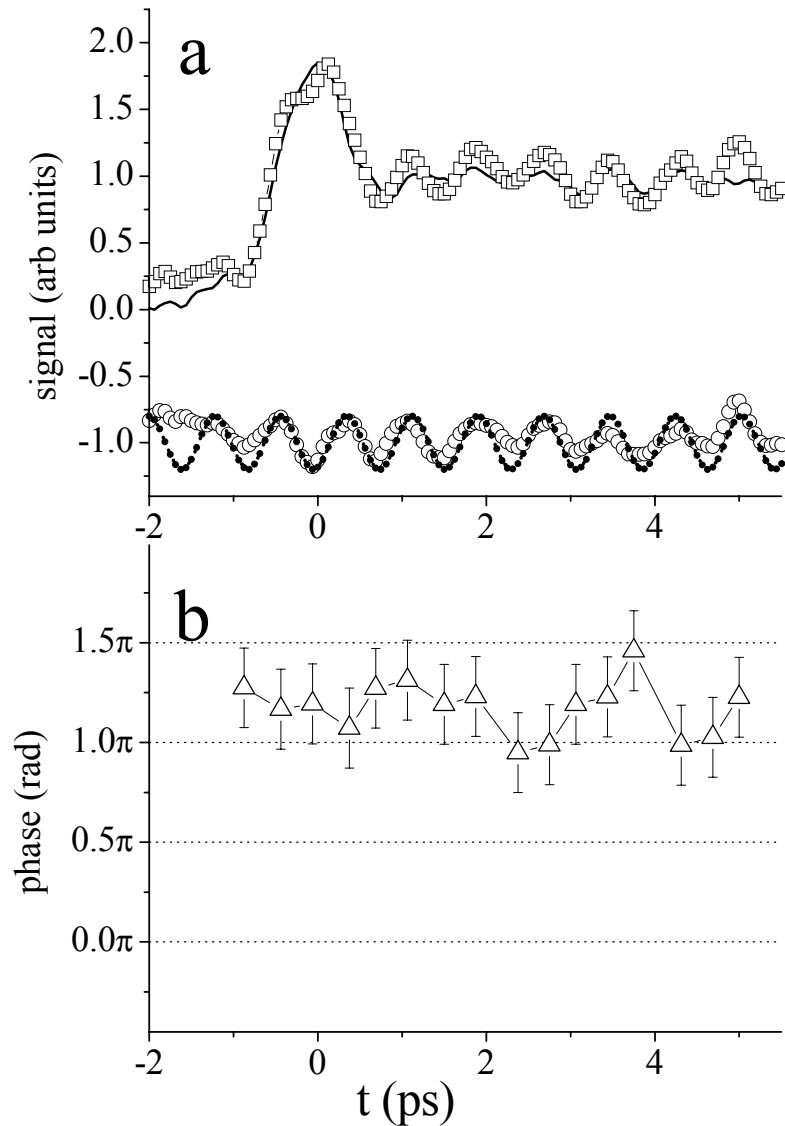


Figure 5.4. Phase evolution using the same phase mask for each resonance. Panel a: Pump-probe signals using phase mask of Fig. 5.2. Total signal ( $\square$ ) and population transfer (solid line) traces are shown on the top. Also shown is the coherence-only signal ( $\circ$ ) as well as a single cosine fit (dotted line). The coherence-only signal and fit have been vertically offset for visibility. Panel b: Instantaneous wave packet phase. The maxima and minima of the coherence-only signal are compared to the fit to generate the instantaneous phase. The wave packet phase remains relatively constant from the onset of the signal until long times.

To show that the phase of the wave packet oscillation remains constant during the population transfer process, the signal up to 6.0 ps pump-probe delay was compared to a cosine wave that is generated to fit the coherence signal between  $t=6$  ps and  $t=30$  ps. The signal is fit only at times after 6 ps to avoid potential uncertainties introduced by a changing wave packet phase during the population transfer process. The maxima and minima of the coherence signal are compared to the fit, and the time offset of each peak relative to the fit is used to determine the instantaneous phase, plotted in Fig. 5.4b. As is evident in Fig. 5.4b, the phase shift of the experimental trace is centered around  $1.16\pi \pm 0.25\pi$  (maximum range) radians over all time delays up to 6 ps. This comes as no surprise, since no effects have been introduced to change the instantaneous wave packet phase.

The case of subtracting the nonresonant contributions from the resonant contribution is the main point of this paper and is shown in Fig. 5.5. The phase mask that is used to induce a sign change in state  $|2\rangle$  is shown in Fig. 5.5a. Note that the phase applied to the nonresonant contributions around  $|1\rangle$  is not changed from the additive case, as shown in the previous section. In contrast, the phase applied to the nonresonant contributions around  $|2\rangle$  is inverted; the nonresonant contributions have an additional  $\pi$  phase shift relative to the resonant ones, which is equivalent to a multiplication by -1, as explained previously. The corresponding signal traces from Fig. 5.5b show the expected population peak around  $t=0.0$  ps, just as when the contributions were added together. Note that this trace must remain positive, since the observed signal is a sum of squares for

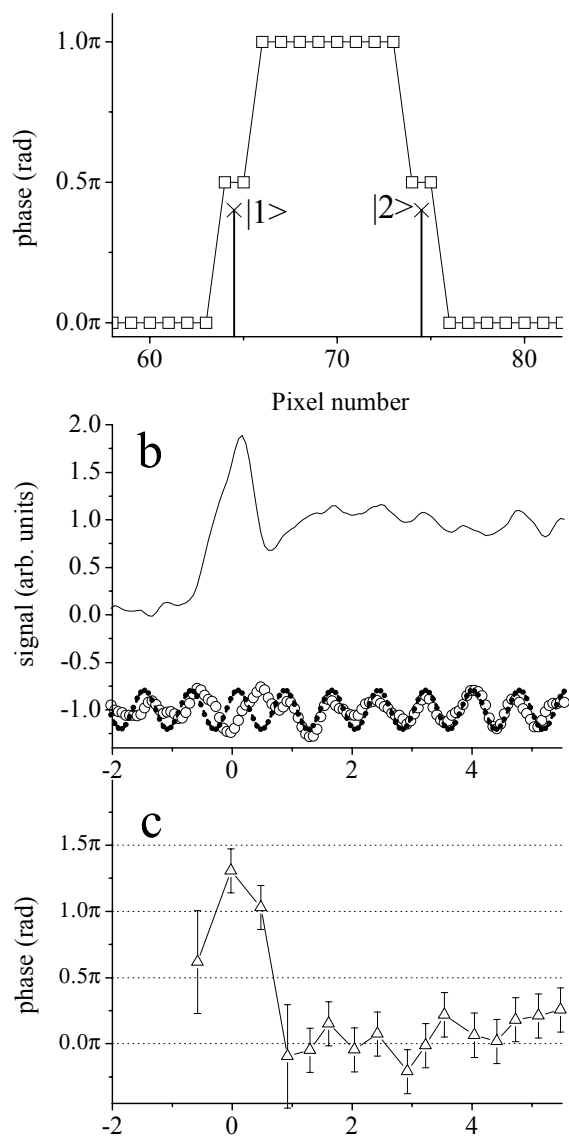


Figure 5.5. Sign inversion wave packet data. State  $|1\rangle$  is programmed to behave the same as in Fig. 5.4, but state  $|2\rangle$  is programmed to change sign. Panel a: Phase mask applied to induce sign inversion. The applied phase is given as ( $\square$ ), and the resonances are given by (X). Notice that the relative phase between resonances is  $0.0$  radians. Panel b: Pump-probe signals using the phase mask of panel a. Population transfer (solid line) trace is shown in addition to the coherence-only signal ( $\circ$ ) as well as a single cosine fit (dotted line). The coherence-only signal and fit have been vertically offset for visibility. Panel c: Instantaneous wave packet phase from onset of excited state population. The wave packet phase undergoes a  $\pi$  shift from  $t=0.0$  ps to  $t>1.0$  ps.

both states  $|1\rangle$  and  $|2\rangle$ . A critical difference in this case occurs in the coherence only portion of the signal, which contains information about the wavefunction sign. In Fig. 5.5b it is apparent that around  $t=0.0$  ps, the quantum beat portion of the signal exhibits a phase of  $\sim\pi$  even though the relative phase between the resonant frequencies is 0.0 radians. The instantaneous phase graph of Fig. 5.5c displays a  $\pi$  phase shift in the region around  $t=0.0$  ps relative to  $t>2.0$  ps. This shows that there is indeed a temporally dynamic phase of one state in the wave packet relative to the other. In fact, it shows that the sign of one state has changed temporarily relative to the other.

A full discussion of the effects seen here can not be made without a brief mention of the nonidealities at play in this pulse shaping scheme. As was mentioned earlier, the resonant contribution to the signal was shifted to a more positive time to minimize the interactions between it and the nonresonant contributions. An example when the nonresonant contribution to the signal is not shifted in time is shown in Fig. 5.6. It is quite clear in this figure that the phase deviates substantially from either 0 or  $\pi$  phase. The dynamics at play here are highly sensitive to the positions of the resonances relative to the cutoffs between those spectral regions treated as “resonant” and “nonresonant.” Within the “resonant” portion of the bandwidth, there are variable amounts of positive and negative detuned wavelengths that have no compensating phase added. The net effect of this is that the instantaneous phase of the nonresonant contribution is not necessarily zero or  $\pi$ . When this nonideality interacts with the transiently prepared state, there can be a large shift in instantaneous phase, as demonstrated

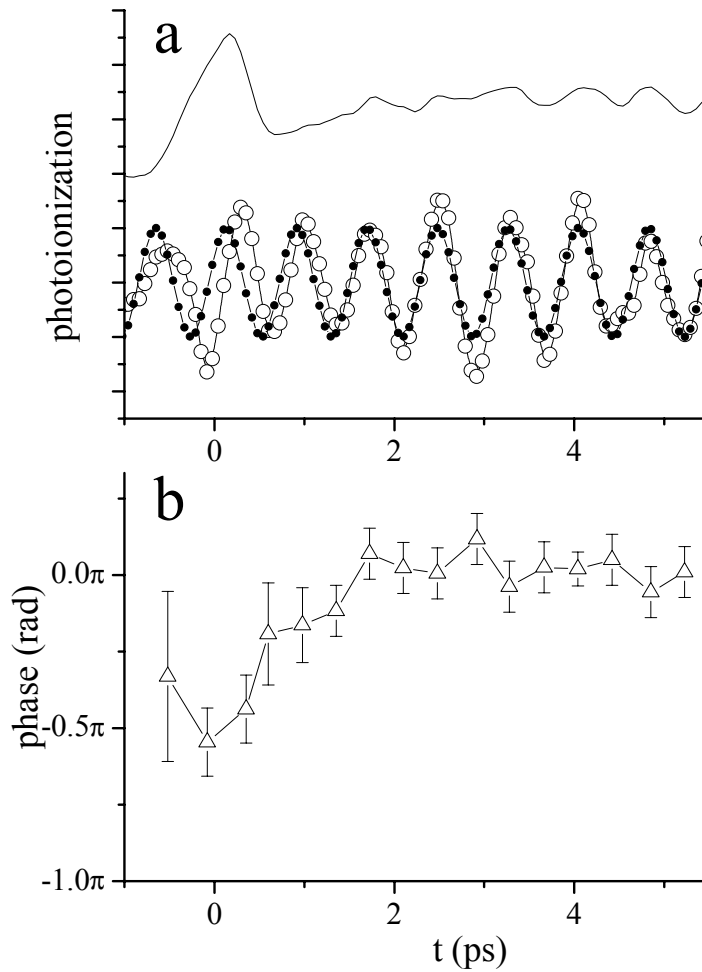


Figure 5.6: Sign inversion wave packet data without time-shifting the resonant contribution. All symbols are the same as Fig. 5.5. Notice the deviation in instantaneous phase away from 0 or  $\pi$  phase at short times. Also notice that the oscillation amplitude fails to approach zero between 0.0 and 2.0 ps.

in Fig. 5.6b. For this reason, the instantaneous phase is most predictable as the resonant and nonresonant contributions are separated in time.

Around  $t=0.0$  ps, when the sign of the wave function for state  $|2\rangle$  is inverted from that expected for the purely resonant phases, there is a certain degree of destructive interference in the contributions to the signal. By performing Wavelength Subtraction Spectroscopy (WSS) with the shaped pulses, a measure of the relative contributions of the various spectral contributions can be made. The traces shown in Fig. 5.7 illustrate destructive interference at play around  $t=0.0$  ps for state  $|2\rangle$ . The data were acquired by setting the pump-probe delay to a specific time delay, either 6.0 ps or 0.0 ps, with either unshaped or shaped pulses, respectively, and attenuating the light imaged onto one pixel at a time. The circles in Fig. 5.7 show the WSS spectrum for unshaped pulses at a pump-probe time delay of 6.0 ps. The trace shows a narrow bandwidth of contributing pixels, as one would expect since resonant frequencies determine the ultimate behavior of each state at long times in the weak field limit. The approximately two-pixel bandwidth is primarily an effect of spot size on the pulshaper and not intrinsic transition bandwidth.

The squares show the spectral contributions to the signal at  $t=0.0$  ps for both states  $|1\rangle$  and  $|2\rangle$  using the phase mask of Fig. 5.5a. The overall lineshape for state  $|1\rangle$  only partially reflects the  $1/\Delta$  behavior expected from Eq. (4.2), but it unambiguously shows an increase in the contributing bandwidth. The increase in effective bandwidth is attributed to the application of  $\pm \pi/2$  phase to positively and negatively detuned frequencies. The spectral asymmetry is a result of a

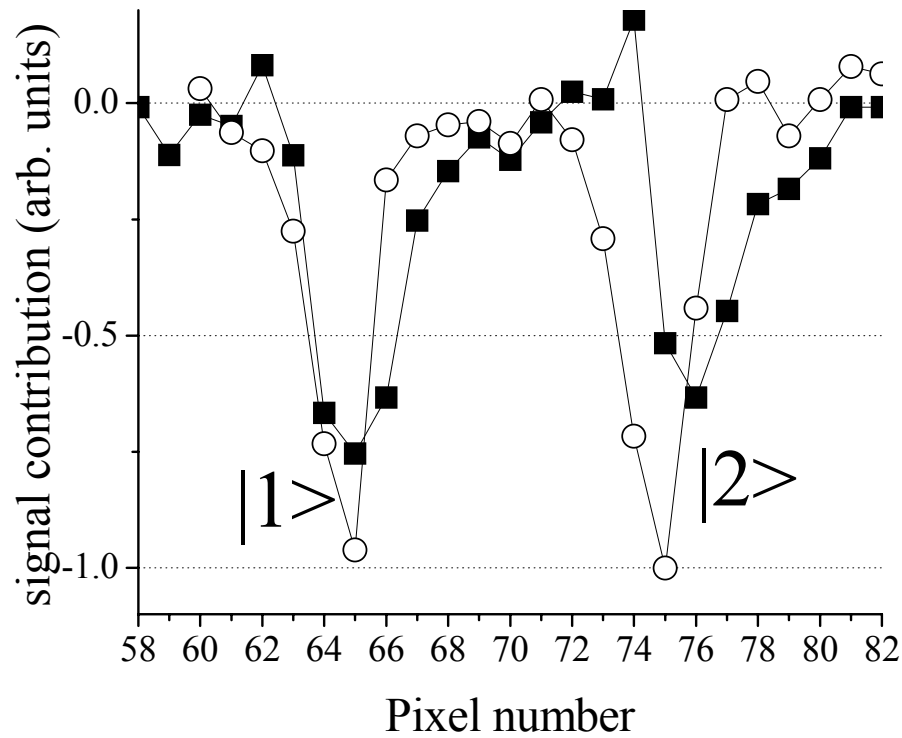


Figure 5.7: Wavelength Subtraction Spectroscopy traces for shaped and unshaped pulses. Here, the signal reflects the change in photoionization relative to background. The (○) is the WSS photoionization spectrum for an unshaped pulse at a fixed pump-probe delay of greater than 6.0 ps. The observed linewidths represent the resolution of the pulse shaper. The (■) show the WSS photoionization spectrum for the phase mask of Fig. 5.5a at a fixed pump-probe delay of 0.0 ps. The (■) spectrum around pixel 65 shows the effect of adding resonant and nonresonant contributions, and that around 75 represents subtracting resonant from nonresonant. Note the increased linewidth of the shaped pulses, and the increase in signal while blocking pixel 74.

combination of diffraction effects in the SLM and an asymmetric laser pulse spectrum. The WSS spectrum at  $t=0.0$  ps for state  $|2\rangle$  similarly shows that there is an increase in the contributing bandwidth relative to the long time delay. More interestingly, the results show that blocking the resonant wavelength actually increases the signal at  $t=0.0$  ps, indicating a destructive interference. Even though the lineshape remains ambiguous, the increase in signal by blocking the resonant frequency on pixel 74 relative to the baseline is unambiguous. Since the wave packet signal at long times consists of recurrence oscillations with a phase offset of approximately zero, the resonant contribution to the signal can be concluded to have a positive sign relative to state  $|1\rangle$ . This suggests that the total wave function coefficient for state  $|2\rangle$  around  $t=0.0$  is negative, in agreement with the wave packet phase data.

The results can be quantified in terms of the  $Z$ -gate representation as in Eq. (5.3), with the initial state taken to be the superposition at  $t=0.0$  ps, and the final state taken to be the superposition at  $t=\infty$ :

$$\begin{bmatrix} c_1(f) \\ c_2(f) \end{bmatrix} = \begin{bmatrix} \frac{res_1(\infty)}{res_1(0) + nonres_1(0)} & <.1 \times res_1(\infty) \\ <.1 \times res_1(\infty) & \frac{res_2(\infty)}{res_2(0) - nonres_2(0)} \end{bmatrix} \begin{bmatrix} c_1(i) \\ c_2(i) \end{bmatrix}, \quad (5.4a)$$

where  $res_i(t)$  and  $nonres_i(t)$  are the resonant and nonresonant contributions to state  $i$  at time  $t$ . The off diagonal elements are a result of cross-talk between control channels which have previously been quantified with respect to the resonant contribution to the coefficients[33]. These off diagonal elements are essentially a measure of the degree to which the dynamics of each state can be independently

controlled. The diagonal elements of Eq. (5.4a) can be taken directly from the experimental data. The first diagonal element is determined to be 0.71, based upon the data from Fig. 5.2. The second diagonal element can be determined from the coherent oscillation amplitude shown in Fig. 5.5. Around  $t=0.0$  ps, the peak-to-peak amplitude of the coherent oscillation is approximately 1.1 times greater than that at long time delays. Given that the coherent oscillation amplitude is proportional to  $|c_1||c_2|$ , and that  $|c_1| \approx 1.4$ , then  $|c_2(t=0)| \approx 0.79|c_2(t=\infty)|$ . This gives a value of -1.3 for the second diagonal element of the transient Z-gate matrix, to yield an experimental transformation of

$$\begin{bmatrix} c_1(f) \\ c_2(f) \end{bmatrix} = \begin{bmatrix} 0.7 \pm 0.2 & <.1 \\ <.1 & -1.3 \pm 0.2 \end{bmatrix} \begin{bmatrix} c_1(i) \\ c_2(i) \end{bmatrix}. \quad (5.4b)$$

Ideally, as long as a phase of  $\pm \pi/2$  is applied to the various nonresonant contributions to the wave packet, there will only be an addition or subtraction of those components relative to resonance, so the matrix components in this case can be assumed to have very little imaginary component. In other words, all contributions to the signal have been manipulated to have phases of either zero or  $\pi$ , which lie along the real axis of the complex plane. Experimentally, we observe the phase to be centered around zero or  $\pi$ , but limitations in the instantaneous phase detection introduce substantial error, see Fig. 5.5.

The instantaneous wavefunction phase could be better controlled and determined if the energy spacing between states were greater. The ability to control one state versus another increases as the state spacing increases as a result of the intrinsic  $1/\Delta$  Rabi oscillation amplitude of Eq. (4.2)[33]. In the current

case, state  $|1\rangle$  is used for a type of heterodyne detection of the phase of state  $|2\rangle$ , where the first state is used to serve as a reference for the second. The interference between  $|1\rangle$  and  $|2\rangle$  permits effective viewing of the phase of state  $|2\rangle$ , but only at the maxima and minima of the interference signal, giving a data point every  $2/\omega_{12}$  ps, where the state spacing  $\omega_{12}$  is given in units of THz. With the current state spacing of  $42\text{ cm}^{-1}$ , one data point is retrieved every 0.3 ps, which is nearly half of the timescale over which the phase of state  $|2\rangle$  changes from  $\pi$  to 0 radians. Increasing the state spacing, or increasing the coherent oscillation frequency, will provide a more accurate probe for how the phase change occurs. Additionally, a more rapid coherent oscillation will provide a more accurate amplitude of the coherent oscillation.

In this chapter, we outlined a system for temporarily switching the relative sign of one state in a superposition while keeping the sign of a second state constant. We showed that this can be done by simply using weak field, phase shaped ultrafast pulses. Additionally, we showed, using established spectral techniques, that the resonant and nonresonant contributions to a specific transition can be programmed to add together or to work in opposition on short timescales. This work expands upon established methods for controlling transient processes in molecular systems and presents a case where both the phase and amplitude of an excited state depend upon more than resonant frequencies.